High-sensitivity high-throughput chip based biosensor array for multiplexed detection of heavy metals

Hai Yan[a,*], Naimei Tang[b], Grace A. Jairo[c], Swapnajit Chakravarty[b], Diane A. Blake[c], and Ray T. Chen[a,b,*]

[a]Department of Electrical and Computer Engineering, The University of Texas at Austin, Austin, TX 78758, USA;

[b]Omega Optics Inc., 8500 Shoal Creek Blvd., Austin, TX, 78759, USA;

[c]Department of Biochemistry and Molecular Biology, Tulane University School of Medicine, New Orleans, LA 70112, USA

ABSTRACT

Heavy metal ions released into the environment from industrial processes lead to various health hazards. We propose an on-chip label-free detection approach that allows high-sensitivity and high-throughput detection of heavy metals. The sensing device consists of 2-dimensional photonic crystal microcavities that are combined by multimode interferometer to form a sensor array. We experimentally demonstrate the detection of cadmium-chelate conjugate with concentration as low as 5 parts-per-billion (ppb).

Keywords: photonic crystals, optical microcavities, optical biosensors, multimode interferometer, cadmium, silicon waveguides.

*hai.yan@utexas.edu, raychen@uts.cc.utexas.edu

1. INTRODUCTION

Silicon photonic biosensors belong to a type of integrated device that possesses the advantages of high-sensitivity, label-free detection of biomolecules and the potential to achieve high integration density and low cost due to its small footprint and CMOS compatible fabrication process. Over the last two decades, silicon photonic biosensors have become a rapidly growing research topic. Various devices, including surface plasmon devices [1][2], microring resonators [3][4], silicon nanowires [5], nanoporous silicon waveguides [6], Bragg gratings [7], one-dimensional (1D) and two-dimensional (2D) photonic crystal (PC) microcavities [8][9], have been demonstrated. The 2D PC cavity sensors take advantage of their slow light enhanced sensitivity within a miniature footprint and thus are able to detect very low concentrations down to atto-gram levels[10].

Heavy metal ions released into the environment via industrial activities cause persistent environmental issues that lead to various health hazards. Cadmium, lead and mercury metal ions are typical examples among those highly dangerous substances. Cadmium is believed to have a biological half-life of more than 15 years in the human body [11]. Recently, immunoassay-based detection approach for cadmium has been proposed and the antibody that recognizes cadmium-chelate complexes has been developed and demonstrated[12].

In the paper, we propose a multi-channel biosensor array consisting of PC microcavity biosensors for the detection of cadmium-chelate conjugate. The PC microcavity biosensors are combined by multimode interferometer (MMI) power splitter. Two types of PC microcavites we demonstrated previously are used: the L13 PC microcavity formed by 13 missing holes in the Γ-K direction and the L13 with nanoholes PC microcavity formed by adding defect holes in the L13 PC microcavity to enhance the mode overlap with biosamples. The biosensor array we proposed here can potentially be used to detect multiple antibody-antigen interactions with high sensitivity, high throughput and without the need for labelling.

Frontiers in Biological Detection: From Nanosensors to Systems VIII, edited by Benjamin L. Miller, Brian T. Cunningham, Amos Danielli, G. Logan Liu, Sharon M. Weiss Proc. of SPIE Vol. 9725, 972507 · © 2016 SPIE · CCC code: 0277-786X/16/$18 · doi: 10.1117/12.2212731

2. DEVICE DESIGN AND FABRICATION

Schematic of the proposed biosensor array is shown in Fig. 1(a). Four PC biosensors were combined in an MMI power splitter to allow for simultaneous test. Subwavelength grating couplers were used to couple CW light in and out of the waveguide devices [13]. Microfluidic channels are integrated on the chip to flow biosamples onto the surface of each sensor.

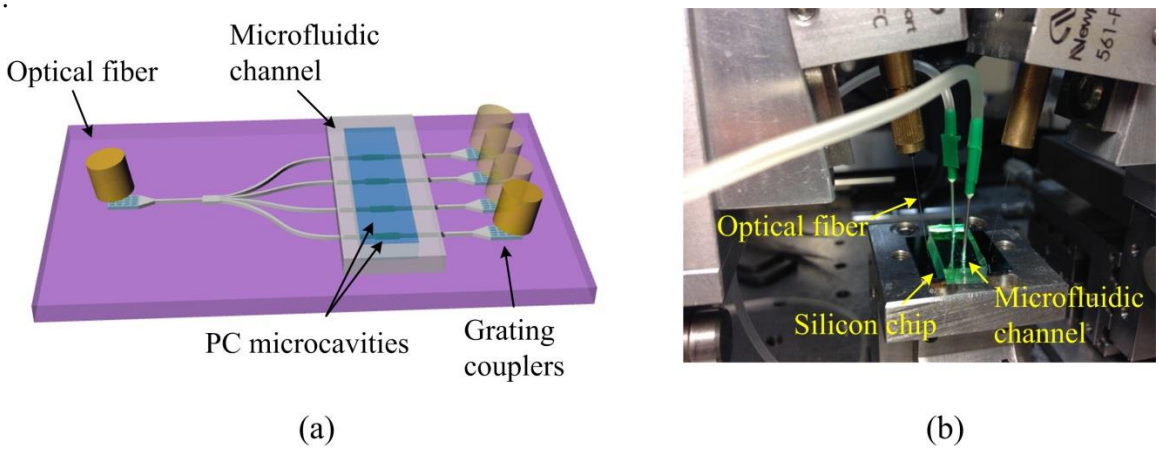

Figure 1. (a) Schematic of a biosensor array consisting of four photonic biosensors on the same chip; (b) Optical testing setup with optical fibers coupled to silicon chip vertically through grating couplers; microfluidic channels are also integrated in the setup.

The devices were fabricated on a silicon-on-insulator (SOI) wafer with e-beam lithography process followed by reactive ion etch. We have previously demonstrated that the same devices can also be fabricated by 193nm UV photolithography in a commercial foundry[14]. The lattice constant of the PC are designed as a = 392.5 nm and the air holes have a radius of r = 108 nm. In L13 with nanoholes device, the nanoholes have a radius of 0.4r = 43 nm. Fig. 2(a) shows a microscope image of the MMI and the four optical channels. Waveguide crossings are introduced on both sides of the PC biosensors, to prevent leakage of liquid from the microfluidic channels. Because the silicon strip waveguides are formed by etching air trenches along both sides of the waveguides, when putting microfluidic channels on top of the biosensors, a leaking path is formed in the trenches. The waveguide crossings serve as a block to seal the trenches and prevent leakage[15]. Scanning electron microscope (SEM) image of the waveguide crossings is shown in Fig. 2(a). Fig. 2(b) and (c) are SEM images of the L13 with nanoholes PC biosensor and the subwavelength grating, respectively.

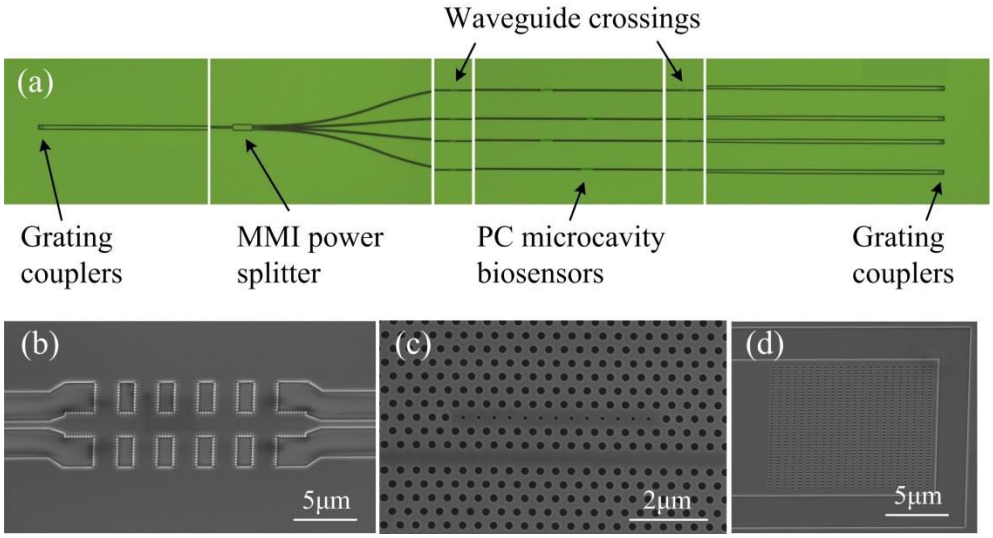

Figure 2. (a) Microscopic image of the fabricated 4-channel PC biosensor array; (b)-(d) Scanning electron microscope images of the (b) waveguide crossings, (c) PC microcavity biosensor (L13 with nanoholes shown) and (d) subwavelength grating couplers.

3. RESULTS

The fabricated device was tested with an optical testing setup that is integrated with microfluidic channels, as shown in Fig. 1(b). Light from a broadband amplified spontaneous emission (ASE) source (1510 nm-1630 nm) is coupled into the sensor chip to excite fundamental transverse-electric (TE) mode in the waveguide. Output light signal is coupled into an optical spectrum analyzer (OSA) to generate the optical spectrum. Microfluidic channel made of polydimethylsiloxane (PDMS) is sealed on the chip to flow biosamples onto the biosensor surface.

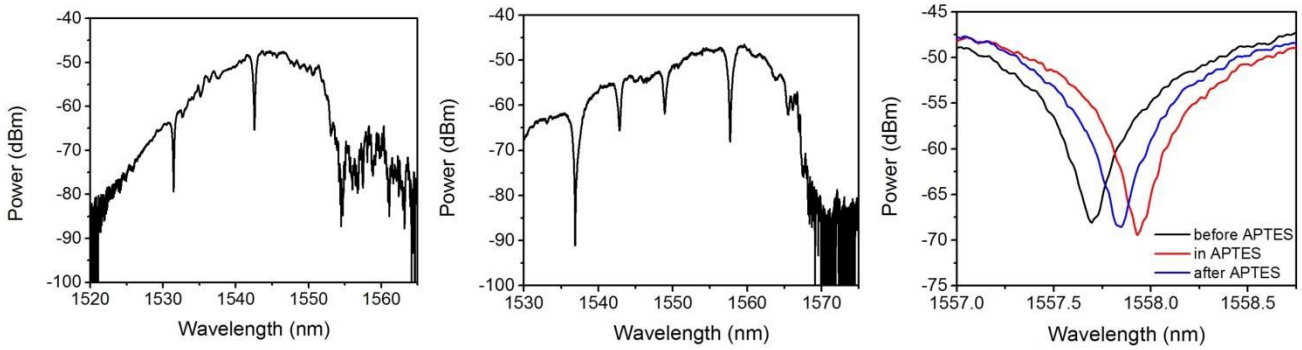

Figure 3. (a) Optical spectrum of an L13 with nanoholes PC microcavity; (b) Optical spectrum of an L13 PC microcavity; (c) Optical spectra of one of the resonances of an L13 PC microcavity at different steps of the experiment, showing the resonance shift.

The optical spectra of the biosensor are characterized first. Fig. 3(a) and (b) show the output spectra of the two types of PC biosensors used in the test: the L13 with nanoholes PC microcavity and the L13 PC microcavity, respectively. Several clear resonance dips were observed in both spectra. The abrupt power drop at the right side of the spectra indicate the PC band edge above which the guided modes are no longer supported, resulting in high propagation loss. We chose the resonance dip closest to the band edge in both biosensors (at 1542.5nm for L13 with nanoholes, and 1558 nm for L13) to take advantage of the slow light effect. Fig. 3(c) shows an example of the resonance shift in the L13 PC sensor at different steps of the experiment. In this way, we were able to detect the target biomolecules binding to specific antibody that was immobilized on our sensor surface.

In order to covalently immobilize the antibody on the sensor surface, the silicon chip was treated chemically by flowing 3-aminopropyl-triethoxy-silane (APTES, 5% in ethanol) and glutaraldehyde (1.25% in phosphate buffered saline (PBS)). During the process, the resonance wavelength in L13 PC sensor was monitored every two minutes and the resonance shift versus time is plotted in Fig. 4(a) and (b). In Fig. 4(a), ethanol was first flowed in to create a baseline. When APTES was flowed in subsequently, a red shift was observed due to a combined effect of bulk refractive index change and the surface area mass change from the attached chemical groups. During the incubation, the curve rose to a saturation level. After washing with ethanol, there is a net resonance wavelength shift of about 0.14 nm, indicating the successful binding of amine groups from APTES. Fig. 4(b) shows similar trend for glutaraldehyde treatment where aldehyde groups were generated on the surface of the chip.

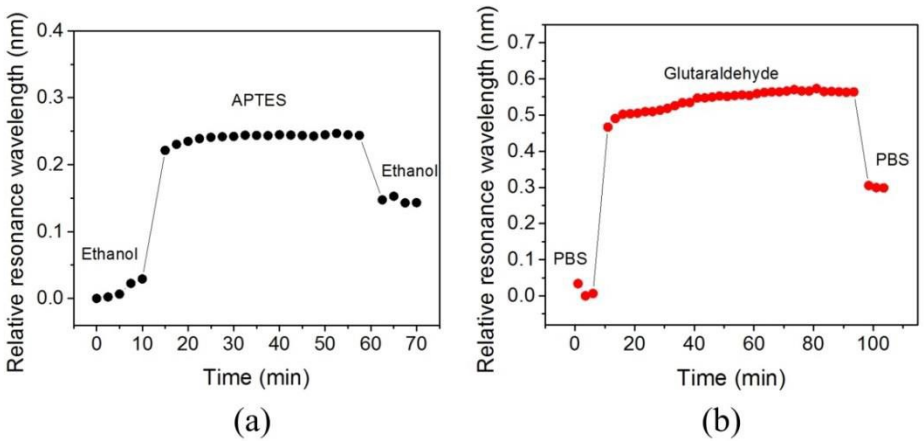

Figure 4. Real-time resonance shift monitoring during the surface treatment of the silicon sensor chip with (a) APTES and (b) glutaraldehyde.

After the above surface treatment, the chip is ready to immobilize probe antibodies. Goat anti-mouse polyclonal antibody and 2A81G5 monoclonal antibody (both in 50 μg/mL) were flowed in the microfluidic channel sequentially. Then 3% bovine serum albumin (BSA) was introduced to saturate the surface and prevent any unspecific binding of target molecules. Fig. 5(a) shows the resonance shift after the above three steps with respect to a same baseline. The shifts indicate that the probe antibodies have been successfully immobilized on the sensor surface and that the vacant binding sites have been covered by BSA.

Finally, target solutions containing different concentrations of cadmium-EDTA-BSA were introduced into the channel and the resonance shifts were recorded for both L13 and L13 with nanoholes biosensors. The results are shown in Fig. 5(b). For both sensors, there was negligible shift for negative control sample, where there is no cadmium in it. With increased concentration from 5ppb to 500ppb, the shift in L13 increased consistently. There is also increased shift in L13 with nanoholes from 5ppb to 50pppb, but the shift drops at the 500ppb probably due to accidental introduction of air bubbles in the channel when the device was being tested. As expected, the shift values for L13 with nanoholes are significantly higher than the L13 sensor because the nanoholes enhance the mode overlap with the biomolecules [8].

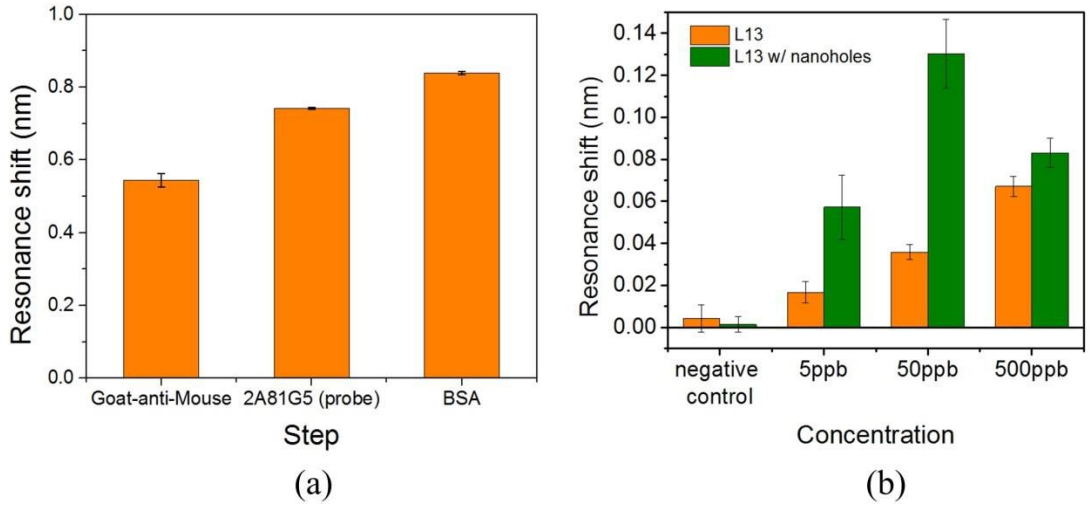

Figure 5. (a) Resonance shift of the L13 PC biosensor for antibody immobilization and BSA blocking steps with respect to a same baseline; (b) Resonance shift of the L13 and L13 with nanoholes PC biosensor after applying increasing concentration of cadmium samples.

4. SUMMARY

In summary, we demonstrated the detection of cadmium-EDTA-BSA conjugate down to 5ppb with an on-chip biosensor array consisting of L13 and L13 with nanoholes PC microcavity biosensors. This type of silicon photonic biosensor array is promising in label-free, high-sensitivity and high-throughput biosensing applications.

ACKNOWLEDGEMENT

The authors would like to acknowledge the US Department of Energy for supporting this work under Grant #DE-SC0013177.

REFERENCES

[1] Yanik, A. A., Huang, M., Artar, A., Chang, T. Y.., Altug, H., "Integrated nanoplasmonic-nanofluidic biosensors with targeted delivery of analytes," Appl. Phys. Lett. **96**(2) (2010).
[2] Zhang, B., Morales, A. W., Peterson, R., Tang, L.., Ye, J. Y., "Label-free detection of cardiac troponin I with a photonic crystal biosensor," Biosens. Bioelectron. **58**, 107–113 (2014).
[3] Iqbal, M., Gleeson, M. A., Spaugh, B., Tybor, F., Gunn, W. G., Hochberg, M., Baehr-Jones, T., Bailey, R. C.., Gunn, L. C., "Label-free biosensor arrays based on silicon ring resonators and high-speed optical scanning instrumentation," IEEE J. Sel. Top. Quantum Electron. **16**(3), 654–661 (2010).
[4] Schmidt, S., Flueckiger, J., Wu, W., Grist, S. M., Talebi Fard, S., Donzella, V., Khumwan, P., Thompson, E. R., Wang, Q., et al., "Improving the performance of silicon photonic rings, disks, and Bragg gratings for use in label-free biosensing," Proc. SPIE 9166, Biosensing Nanomedicine VII, H. Mohseni, M. H. Agahi, and M. Razeghi, Eds., 91660M (2014).
[5] Janz, S., Xu, D.-X., Vachon, M., Sabourin, N., Cheben, P., McIntosh, H., Ding, H., Wang, S., Schmid, J. H., et al., "Photonic wire biosensor microarray chip and instrumentation with application to serotyping of Escherichia coliisolates.," Opt. Express **21**(4), 4623–4637 (2013).
[6] Wei, X., Mares, J. W., Gao, Y., Li, D.., Weiss, S. M., "Biomolecule kinetics measurements in flow cell integrated porous silicon waveguides.," Biomed. Opt. Express **3**(9), 1993–2003 (2012).
[7] Wang, X., Flueckiger, J., Schmidt, S., Grist, S., Fard, S. T., Kirk, J., Doerfler, M., Cheung, K. C., Ratner, D. M., et al., "A silicon photonic biosensor using phase-shifted Bragg gratings in slot waveguide," J. Biophotonics **6**(10), 821–828 (2013).
[8] Liang, F., Clarke, N., Patel, P., Loncar, M.., Quan, Q., "Scalable photonic crystal chips for high sensitivity protein detection.," Opt. Express **21**(26), 32306–32312 (2013).
[9] Lai, W. C., Chakravarty, S., Zou, Y., Guo, Y.., Chen, R. T., "Slow light enhanced sensitivity of resonance modes in photonic crystal biosensors," Appl. Phys. Lett. **102**(4) (2013).
[10] Chakravarty, S., Hosseini, A., Xu, X., Zhu, L., Zou, Y.., Chen, R. T., "Analysis of ultra-high sensitivity configuration in chip-integrated photonic crystal microcavity bio-sensors," Appl. Phys. Lett. **104**(19) (2014).
[11] Satarug, S.., Moore, M. R., "Adverse health effects of chronic exposure to low-level cadmium in foodstuffs and cigarette smoke," Environ. Health Perspect. **112**(10), 1099–1103 (2004).
[12] Blake, D. A., Chakrabarti, P., Khosraviani, M., Hatcher, F. M., Westhoff, C. M., Goebel, P., Wylie, D. E.., Blake, R. C., "Metal binding properties of a monoclonal antibody directed toward metal-chelate complexes.," J. Biol. Chem. **271**(44), 27677–27685 (1996).
[13] Xu, X., Subbaraman, H., Covey, J., Kwong, D., Hosseini, A.., Chen, R. T., "Complementary metal-oxide-semiconductor compatible high efficiency subwavelength grating couplers for silicon integrated photonics," Appl. Phys. Lett. **101**(3) (2012).
[14] Yang, C.-J.; Zou, Y.; Chakravarty, S.; Yan, H.; Wang, Z.; Chen, R. "*Wide Dynamic Range Sensing in Photonic Crystal Microcavity Biosensors*," CLEO: 2014, San Jose, California, STh4H.5. (2014)
[15] Wang, Z., Yan, H., Chakravarty, S., Subbaraman, H., Xu, X., Fan, D. L., Wang, A. X.., Chen, R. T., "Microfluidic channels with ultralow-loss waveguide crossings for various chip-integrated photonic sensors.," Opt. Lett. **40**(7), 1563–1566 (2015).